



<b>Title</b>	<b>Planar hexagonal meshing for architecture</b>
<b>Author(s)</b>	<b>Li, Y; Choi, YK; Liu, Y; Wang, WP</b>
<b>Citation</b>	<b>IEEE Transactions on Visualization and Computer Graphics, 2015 v. 21 n. 1, p.95-106</b>
<b>Issued Date</b>	<b>2015</b>
<b>URL</b>	<b><a href="http://hdl.handle.net/10722/206081">http://hdl.handle.net/10722/206081</a></b>
<b>Rights</b>	<b>Creative Commons: Attribution 3.0 Hong Kong License</b>

# Planar Hexagonal Meshing for Architecture

Yufei Li, Yang Liu, and Wenping Wang

**Abstract**—Mesh surfaces with planar hexagonal faces, what we refer to as *PH meshes*, offer an elegant way of paneling freeform architectural surfaces due to their node simplicity (i.e., valence-3 nodes) and naturally appealing layout. We investigate PH meshes to understand how the shape, size, and pattern of PH faces are constrained by surface geometry. This understanding enables us to develop an effective method for paneling freeform architectural surfaces with PH meshes. Our method first constructs an *ideal triangulation* of a given smooth surface, guided by surface geometry. We show that such an ideal triangulation leads to a *Dupin-regular* PH mesh via tangent duality on the surface. We have developed several novel and effective techniques for improving undesirable mesh layouts caused by singular behaviors of surface curvature. We compute support structures associated with PH meshes, including exact vertex offsets and approximate edge offsets, as demanded in panel manufacturing. The efficacy of our method is validated by a number of architectural examples.

**Index Terms**—Planar hexagonal mesh, ideal triangulation, mesh offset, architectural geometry

## 1 INTRODUCTION

MESHES with planar faces, i.e., polyhedral meshes, have attracted a great deal of attention recently due to the increasing demand in architecture for modeling freeform surfaces with planar panels [1], [2], [3], [4]. Tiling a surface with planar faces is an extension of the classical plane tiling problem, which has been well studied and reviewed [5]. To tile a plane with only congruent copies of a regular polygon, there are only three possible shape choices: equilateral triangle, square, or regular hexagon (or their affine copies). However, the problem of tiling a surface with the same type of polygons is more challenging. In general, the mesh faces can no longer have identical shapes as they are constrained by the surface geometry. For example, as we shall demonstrate, a negatively curved surface cannot be tiled with a mesh of planar convex polygons that have only valence-3 vertices.

Freeform surfaces in architectural construction are usually rationalized by panels (planar mesh faces) that are framed by beams (mesh edges) joined at nodes/junctions (mesh vertices). A major consideration of the fabrication cost is to reduce node complexity, i.e., vertex valence. Therefore, triangle meshes are not optimal structures because of their high vertex valences. Another disadvantage of triangle meshes is they do not possess exact offsets, which are important for modeling multi-layer structures [6]. These drawbacks motivated the study of meshes with planar quadrilateral faces (PQ meshes). The geometric properties and effective computation methods of PQ meshes have been studied and developed in [2], [6], [7], [8], [9].

A mesh surface with planar hexagonal faces, *PH mesh* for short, is an appealing surface representation for a number of reasons. The hexagonal tiling is omnipresent in nature and is the layout with the tightest circle packing in the plane [10]. Moreover, compared to PQ meshes, PH meshes offer a simple solution for paneling and have a lower fabrication cost because they have the simplest valence-3 nodes and possess the exact face offset property [6], [11], [12]. Finally, PH meshes provide a useful shape representation in discrete differential geometry as their offset property facilitates various surface modeling, e.g., minimal surfaces and constant mean curvature surfaces [3], [13], [14]. Fig. 17 shows two architectural shapes covered by PH panels.

Despite all these advantages, there has been little study in the literature about the geometry or computation of PH meshes. Existing methods for computing PH meshes either work only for simple shapes [12], [15] or do not take into account mesh aesthetics [11], [16], [17], [18] (see Fig. 1-right), which includes mesh fairness, vertex valence regularity (regular vertex in PH meshes has valence 3), and face shape regularity (see Dupin-Regular in Section 3.2). Mesh aesthetics is an important criterion in architectural design. In this paper, we shall investigate the geometry of PH meshes to provide insights into the construction of aesthetic PH meshes for architectural design.

Our contributions are summarized as follows.

- We investigate the geometry of PH meshes by revealing how the shape, size, and pattern of PH faces are constrained by surface geometry and identify the *ideal triangulation* for a given freeform surface that corresponds to an anisotropic regular PH mesh.
- We present a framework for computing such ideal triangulations for given freeform surfaces.
- We provide an effective technique for improving the mesh layout in degenerate regions of a freeform surface, i.e., umbilical and parabolic regions.
- We present methods for computing face offsets, vertex offsets, and approximate edge offsets for PH meshes by optimization.

• Y. Li and W. Wang are with the Department of Computer Science, The University of Hong Kong, Pokfulam Road, Hong Kong, P.R. China. E-mail: liyufei.ustc@gmail.com, wenping@cs.hku.hk.

• Y. Liu is with Microsoft Research Asia, No. 5 Dan Ling Street, Haidian District, Beijing 100080, P.R. China. E-mail: yangliu@microsoft.com.

Manuscript received 8 Oct. 2013; revised 28 Apr. 2014; accepted 2 May 2014. Date of publication 29 June 2014; date of current version 26 Nov. 2014.

Recommended for acceptance by S. Takahashi.

For information on obtaining reprints of this article, please send e-mail to: reprints@ieee.org, and reference the Digital Object Identifier below.

Digital Object Identifier no. 10.1109/TVCG.2014.2322367

## 2 RELATED WORK

*Surface tiling.* Tiling a freeform surface with polygonal faces is an extension of the classic plane-tiling problem. Plane tiling with various patterns is well studied in [5], [10]. For surfaces, polygonal meshes can serve different purposes, such as surface mosaic by quad elements [19], pattern synthesis by hexagonal elements [20], and texture mapping via triangle/quad elements [21]. In these applications, the planarity of the mesh faces is not required in general. However, in architecture, especially when constructing glazed/metal structures, planar panels are important for reducing fabrication costs and complexity [1]. There is a series of works on paneling surfaces with planar quadrilateral faces [2], [4], [9]. Designing and discretizing a conjugate curve network on the surface is the key to successful PQ meshing.

*Planar polygonal meshing.* In addition to PQ meshes, general planar polygonal meshes have recently been introduced in architecture. Cutler and Whiting [11] employed the variational surface approximation approach [22] to compute planar panels for a given surface. The resulting planar polygonal mesh generally contains valence-3 vertices but the approximation quality can be poor and neither the shape nor the number of sides of the faces can be controlled. Pottmann et al. [6] presented an elegant method for computing the dual of a Koebe polyhedron for a planar polygonal mesh. However, their method is a restricted form-finding process and does not work for general shapes. Almegaard et al. [23] computed a piecewise linear supporting function of a surface to construct a PH mesh based on projective duality. These results may contain self-intersecting faces that ruin the aesthetics and utility of the mesh.

For dealing with general freeform surfaces, Troche [16] proposed the construction of PH meshes through tangent duality, i.e., by intersecting tangent planes defined on sample points over the surface. This approach is straightforward and easy to implement, but there are no appropriate rules to guide the sampling of the points, which is important for avoiding hexagonal face self-intersections and interpenetrations. Moreover, the intersection of tangent planes becomes numerically unstable in the parabolic regions or regions of small curvature. To improve the intersection stability and mesh fairness, Zimmer et al. [17] introduced additional degrees of freedom into the tangent plane intersection by formulating it as an optimization problem. Poranne et al. [18] also provided an efficient solver for planarizing the faces of a given polygonal mesh. Both these methods are very effective at producing planar faces yet still have difficulties in achieving mesh aesthetics, although a fairing energy is integrated in the optimization. The reason is that the geometric optimization/planarization based methods can only perturb the vertex positions locally, while the topology (i.e., mesh connectivity) and vertices location of the input mesh plays a more critical role for determining an aesthetic output mesh. For example in Fig. 1, performing the planarization method proposed in [18] on a hexagonal mesh (left) produces a PH mesh (right), where the mesh loses aesthetics and contains irregularly shaped and self-intersecting faces. This indicates that the shape of the PH faces is significantly constrained by the underlying surface geometry, and face

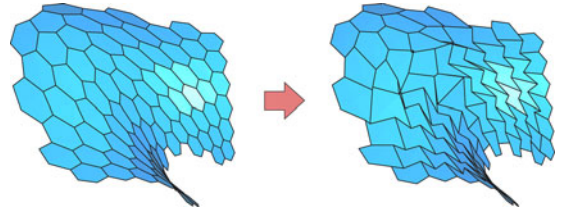


Fig. 1. Left: an input hexagonal mesh with fairing but non-planar faces. Right: a PH mesh obtained by performing the planarization method in [18] on the left input.

planarity and mesh aesthetics might be contradicting goals if the given surface is not properly discretized.

To explicitly control the shape of PH faces, Wang et al. proposed the concept of Dupin duality for studying the relationship between triangular meshes and PH meshes in their technical report [12]. They first sample a triangle mesh from a conjugate curve network, then dualize the triangle mesh to a PH mesh using Dupin duality and planarity optimization. The main limitations of their methods are: (1) they only work for simple surface shapes due to the use of a progressive sampling strategy; (2) the design and mesh layout of the conjugate curve network are missing, which is important to the quality of the resulting PH meshes; (3) the choice of the step size in handling parabolic region requires careful design; (4) the method is not able to deal with free-form surfaces with umbilical regions. Wang and Liu also propose another method for generating a PH mesh from a conjugate curvature network directly in [15]. However, their method also suffers the above problems. In this paper, we overcome these issues by proposing ideal triangulation and developing novel techniques to improve the mesh aesthetic in parabolic and umbilical regions.

*Parallel mesh and mesh offset.* In architectural construction, torsion-free nodes and beams are preferable for easy fabrication. Pottmann et al. [6] presented an elegant concept—*parallel mesh* to achieve torsion-free structures. Mesh parallelism means that two meshes have the same connectivity and the corresponding edges are parallel to each other. Mesh parallelism is closely related to discrete differential geometry [8] and provides the basis for deriving several kinds of offset meshes, such as vertex offset, face offset, and edge offset.

## 3 PH FACES WITH DUPIN-REGULARITY

In this section, we first investigate how the shape of PH faces is constrained by the underlying surface geometry and introduce the optimal shape for PH faces under these constraints. Then, by studying the local property of tangent duality, we identify the ideal triangles that correspond to Dupin-regular PH faces under the tangent duality transformation.

### 3.1 Constrained Shapes of PH Faces

An important concept in our investigation is the *Dupin indicatrix* [24]: given a surface  $S$  and a point  $p \in S$ , the Dupin indicatrix is the collection of conics defined by  $\kappa_1 x^2 + \kappa_2 y^2 = \pm 1$ , where  $\kappa_1, \kappa_2$  are the principal curvatures of  $S$  at  $p$  (Fig. 2-left). As shown in Fig. 2-middle, the Dupin indicatrix is an ellipse when the Gaussian curvature  $K = \kappa_1 \kappa_2 > 0$  at  $p$ , or a

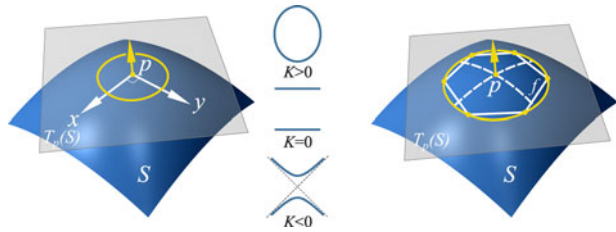


Fig. 2. Dupin indicatrix. Left: A point  $p$  and its tangent plane  $T_p(s)$  on surface  $S$ . The gray plane (which is near and parallel to  $T_p(s)$ ) cuts  $S$  in a Dupin conic. Middle: three possible Dupin conics (ellipse ( $K > 0$ ), parallel lines ( $K = 0$ ), hyperbolic ( $K < 0$ )). Right: a convex hexagon  $f$  at an elliptic point  $p$  inscribed in an ellipse.

pair of hyperbolas when  $K < 0$  at  $p$ , or a pair of lines when  $K = 0$  at  $p$  (assuming  $\kappa_1 \neq 0$  and  $\kappa_2 = 0$ ). Throughout the paper we shall frequently refer to a conic *homothetic* as the Dupin indicatrix. For brevity's sake, we call it a *Dupin conic*, or *Dupin ellipse* or *Dupin hyperbola* if we need to be specific. Thus, with a Dupin conic on surface  $S$  at  $p$ , we mean a homothetic copy of the Dupin indicatrix of  $S$  at  $p$ .

Intuitively, at a point  $p \in S$ , a plane that is near and parallel to the tangent plane  $T_p(S)$  cuts  $S$  in a shape that is in the first-order approximation similar to the Dupin indicatrix [25] in a local region of  $S$  (Fig. 2-left). The face  $f$  is a convex hexagon at an elliptic point of  $S$ , since it is approximately inscribed in an ellipse, and a concave hexagon at a hyperbolic point of  $S$ , since it is approximately inscribed in a hyperbola. Fig. 3 illustrates these cases. The case of  $K = 0$  (i.e., parabolic points) deserves special attention. When the parabolic points are isolated or form a parabolic curve on  $S$ , then the PH face at the point or the curve can assume a variety of shapes, as influenced by the neighboring PH faces where  $K \neq 0$ .

### 3.2 Dupin-Regularity

As discussed, paneling a given surface  $S$  with PH faces is a highly constrained problem and it is difficult to directly discretize  $S$  into a hexagonal tiling that has faces with exact planarity. A natural choice would be to first compute a triangulation  $T$  of  $S$ , and then convert  $T$  to a PH mesh  $H$  via *tangent duality*, as explained below.

Consider a triangle  $t$  of  $T$  with vertices  $v_a, v_b, v_c \in S$ . Then, in general, the three tangent planes of  $S$  at  $v_a, v_b$ , and  $v_c$  intersect at a point. Let us denote this intersection point as  $u_t$  and associate it with triangle  $t$ . If we do this for every triangle  $t$  of  $T$  and connect the points  $u_t$  of triangles adjacent to  $T$ , then we obtain a hexagonal mesh  $H$  combinatorially dual to  $T$ . Clearly, each face of  $H$  is a planar hexagon lying on a plane that is tangent to  $S$  at a vertex of  $T$ . Hence,  $H$  is a PH mesh approximating  $S$ . Conversely, a PH mesh  $H$  with its faces tangent to the surface  $S$  corresponds to a triangle mesh whose vertices are at the tangency points of the faces  $H$  with  $S$ . This correspondence between  $T$  and  $H$  is known as *tangent duality*.

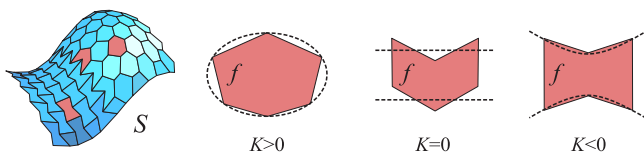


Fig. 3. A PH face approximating  $S$  in an approximation inscribed in a Dupin conic.

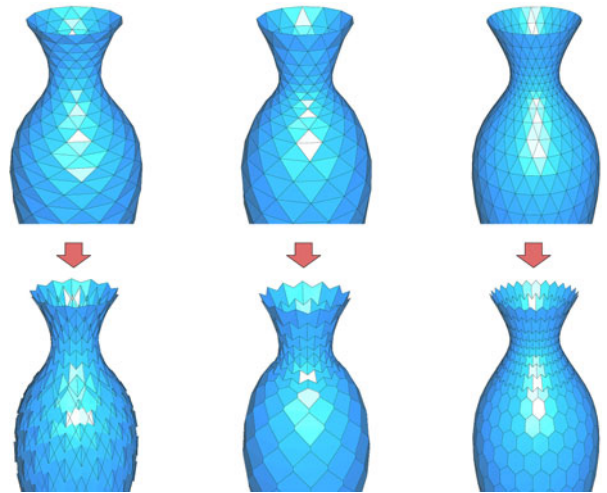


Fig. 4. Three triangulations on the same shape and their corresponding PH meshes under tangent duality. Left: a PH mesh with self-intersecting faces. Middle: a PH mesh with nearly self-intersecting faces. Right: a PH mesh with nicely shaped faces.

Although the tangent duality involves only a straightforward geometric construction, its behavior can be rather complex. Fig. 4 shows three triangulations on the same shape and their corresponding PH meshes under tangent duality. As demonstrated, the faces of a PH mesh may take various shapes, even self-intersecting ones, depending on the layout of the triangulation. Without properly triangulating the surface, the dual PH faces might be of awkward shapes (Fig. 4-middle) or even with self-intersection (Fig. 4-left). These faces would destroy the aesthetics of an architectural design or even make it useless.

A PH face inscribed in a Dupin conic has the flexibility to take various shapes. For hexagonal tiling on a plane, a natural choice is to have the tiles be regular hexagons as much as possible. However, when approximating freeform surfaces, PH faces in general can no longer have the shape of a regular hexagon, as they have to be approximately inscribed in the local Dupin conics as discussed above. Thus, at a point of  $K > 0$ , a natural criterion is to have, as much as possible, a hexagon that transforms into a regular hexagon when scaling the Dupin ellipse back to a circle (Fig. 5b). In the concave case, we introduce the *quasi-regular hexagon* that is formed by juxtaposing the two halves of a regular hexagon (see the upper and lower quadrilaterals of the hexagon in Fig. 5d). Hence, at the point of  $K < 0$ , we would like to have, as much as possible, a hexagon that transforms into a quasi-regular hexagon when scaling the Dupin hyperbola back to a unit hyperbola (Fig. 5d). A PH mesh is called *Dupin-regular*, if its faces are all in the optimal shapes as defined above.

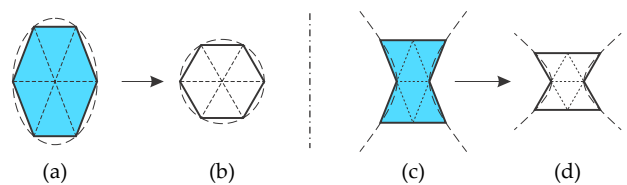


Fig. 5. Left:  $K > 0$ . Right:  $K < 0$ . (a)&(c): Dupin regular hexagons. (b): a regular hexagon. (d): a quasi-regular hexagon.

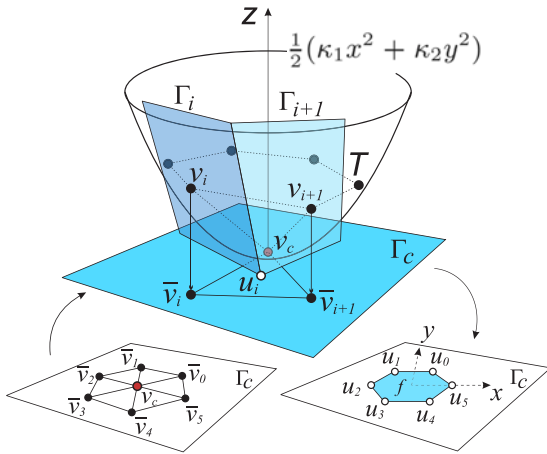
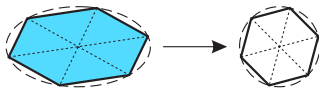


Fig. 6. Tangent duality on the local quadratic approximation of  $S$  in the case of  $K > 0$ .

*Remark.* Given a Dupin ellipse, there are infinite choices for a Dupin regular hexagon (see the inset for an example). However, for preserving the features of a surface, in our application we further require the hexagons to be axially symmetric, i.e., aligned with one of the principal directions (e.g., Fig. 5a).



### 3.3 Ideal Triangles

Next, we shall study the local property of tangent duality and identify for a given surface  $S$  the *ideal triangles* that would be dualized to PH faces with the previously defined optimal shapes.

Suppose  $T$  is a triangulation of a smooth surface  $S$  with face size  $O(h)$  ( $h$  is the average edge length). At a vertex  $v_c \in S$  of  $T$  (Fig. 6), we may approximate  $S$  on the tangent plane  $\Gamma_c$  at  $v_c$  by its second order Taylor expansion  $z = g(x, y) \equiv \frac{1}{2}(\kappa_1 x^2 + \kappa_2 y^2)$  with  $O(h^3)$  error, where  $\kappa_1$  and  $\kappa_2$  are the principal curvatures of  $S$  at  $v_c$  associated with the two principal directions along  $x$ -axis and  $y$ -axis, respectively. Consider a centrally symmetric hexagon  $\bar{v}_0\bar{v}_1\bar{v}_2\bar{v}_3\bar{v}_4\bar{v}_5$  on the tangent plane  $\Gamma_c$  with the triangles  $\Delta v_c\bar{v}_i\bar{v}_{i+1}$  congruent to each other,  $i = 0, 1, \dots, 5$  modulo 6 (Fig. 6-bottom left). Let  $\bar{v}_i = g(\bar{v}_i)$ , and denote  $f : u_0u_1u_2u_3u_4u_5$  as the hexagon on the plane  $\Gamma_c$  obtained by applying the tangent duality to the vertices  $v_i$  on  $z = g(x, y)$ , where every vertex  $u_i$  is given by the triangle  $\Delta v_c\bar{v}_i\bar{v}_{i+1}$ .

We conclude that when  $K > 0$  at  $v_c$ , the hexagon  $f$  under tangent duality is a Dupin regular hexagon, if and only if the triangles  $\Delta v_c\bar{v}_i\bar{v}_{i+1}$  ( $i = 0, 1, \dots, 5$  modulo 6) take the shape as shown in Fig. 7-left (see the derivation in the supplemental

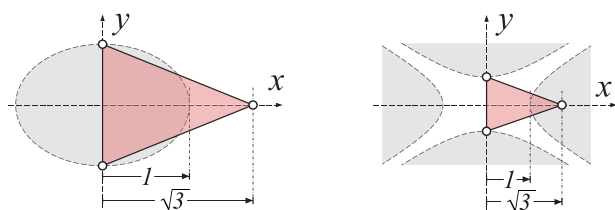


Fig. 7. Ideal triangle in the case of  $K > 0$  (left) and  $K < 0$  (right).

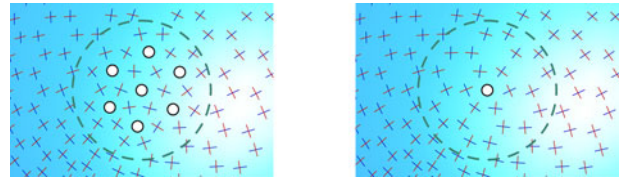


Fig. 8. (Left): The estimation of principal directions becomes numerically unstable in the circled umbilical region, leading to a noisy field with redundant singularities (white dots). (Right): A smooth field with a specified singularity of index  $1/2$  is recovered by optimizing the directions in the umbilical region.

material, which can be found on the Computer Society Digital Library at <http://doi.ieeecomputersociety.org/10.1109/TVCG.2014.2322367>); such a triangle is called an *ideal triangle*. Similarly, when  $K < 0$  at  $p$ , the ideal triangle for obtaining a Dupin quasi-regular hexagon should take the shape as shown in Fig. 7-right. Note that, the shape of an ideal triangle is free up to a uniform scaling, depending on the desired density of the PH mesh. Due to the smoothness assumption on the surface and the second order approximation of the surface, it is easy to see that the vertices of  $T$  that are adjacent to  $v_c$  can be moved to points  $\bar{v}_i$ ,  $i = 0, 1, \dots, 5$ , on surface  $S$ , with a perturbations of  $O(h^2)$ . Thus, in an approximation, the definition of ideal triangles also applies to the triangles of  $T$ .

## 4 COMPUTING AN IDEAL TRIANGULATION

In this section, we present a framework for computing an *ideal triangulation*  $T$  of a given surface  $S$ , whose faces are as close to ideal triangles as possible. An ideal triangulation is in fact an anisotropic triangle mesh with the triangles aligned with principal directions and properly scaled with principal curvatures. To compute such a mesh  $T$  of a discrete surface  $S$ , we need to: (1) compute a smooth and faithful principal direction field of  $S$ ; (2) generate an anisotropic quad mesh aligned with the principal direction field by parameterization; (3) convert the quad mesh into a triangulation containing ideal triangles. These steps will be detailed in the subsequent subsections.

### 4.1 Principal Direction Field

A challenge in computing the principal direction field on a triangulated surface  $S$  is that the estimation of principal directions becomes numerically unstable in the umbilical regions ( $K \approx 0$ ) of  $S$ . This will lead to a noisy and unreliable field with redundant singularities (Fig. 8-left). To handle this problem, we adapt the *trivial connection* method proposed in [26], as it offers full control over field singularities (locations and indices). The basic idea is that the field smoothness can be recovered by re-computing the directions in umbilical regions, which is formulated as a least-square optimization problem. During the optimization, the salient principal directions (where  $\sqrt{|\kappa_{max}|} > 1.5\sqrt{|\kappa_{min}|}$  in our experiments) are fixed as hard constraints. Moreover, for each identified umbilical region of  $S$ , we prescribe a singularity of specific index ( $\frac{1}{2}$  or  $-\frac{1}{2}$ ) at its center according to the type of the umbilical, which is also treated as a hard constraint. The existence of the solution for this linearly constrained least-square problem has been well studied in [26], and it guarantees an as-smooth-as-possible field with faithful singularities and well-preserved salient principal directions (Fig. 8-right).

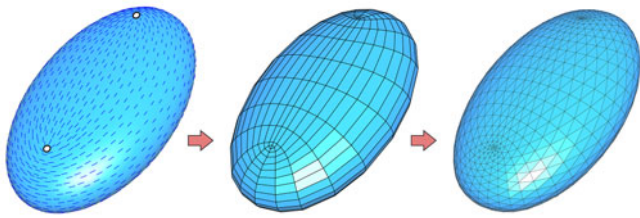
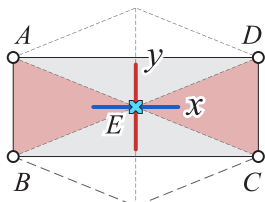


Fig. 9. Computing an ideal triangulation. (Left): A smooth and faithful principal direction field is computed on an ellipsoidal shape. (Middle): An anisotropic quad mesh aligned with the principal direction field is computed by means of surface parameterization. (Right): The quad mesh is converted into a triangulation.

In this paper, for a principal direction field, we assume there are two kinds of singularities, i.e., umbilical points, with index  $\frac{1}{2}$  and  $-\frac{1}{2}$ , respectively. High order singularities [27] are rare and we assume they do not appear. Thus, it is always possible to de-couple the principal direction field into two smooth *line fields*, which are locally orthogonal to each other. We may choose one of them as the direction to scale the triangles (e.g., the  $x$ -axis in Fig. 7), i.e., to align the PH faces. Fig. 9-left shows such a line field computed by our method on an ellipsoidal shape.

## 4.2 Anisotropic Quad Meshing

Next, we construct an anisotropic quad mesh  $Q$  of  $S$  by means of global parameterization similar to [7], [9], [28], [29], [30], i.e., a piecewise linear map from the input triangle mesh to some disk-like parameter domain, which assigns a  $(u, v)$  parameter value for each vertex of the mesh.



The edges of  $Q$  should be aligned with the computed principal direction field, and the faces of  $Q$  should take a proper aspect ratio so that they can split into two ideal triangles in the next step. See the inset for such a quad face. Clearly, the quad face  $ABCD$  can split into two ideal triangles  $\triangle ABE$  and  $\triangle CDE$ , if  $\sqrt{3}|\kappa_2|||AB|| = \sqrt{|\kappa_1|||BC||}$ , where  $\kappa_1$  and  $\kappa_2$  are the principal curvatures of  $S$  at  $E$  associated with the principal directions. When constructing such a  $Q$ , the gradients of the two piecewise linear scalar fields  $u$  and  $v$  should minimize the energy:

$$E_f = \|h\sqrt{|\kappa_1|}\nabla u - \mathbf{n}\|^2 + \|h\sqrt{3|\kappa_2|}\nabla v - \mathbf{n}^\perp\|^2,$$

for each face  $f$  of the input triangle mesh. Here  $h$  is a global scaling parameter that controls the edge length of the resulting quad mesh. The unit vector  $\mathbf{n}$  is the line direction in  $f$  and  $\mathbf{n}^\perp$  is the counter-clockwise rotation of  $\mathbf{n}$  by 90 degrees in the plane of the face  $f$ , and  $\kappa_1$  and  $\kappa_2$  are the principal curvatures at  $f$  associated with  $\mathbf{n}$  and  $\mathbf{n}^\perp$ , respectively, representing anisotropy. The minimization of the energy  $E_T = \sum_f \text{area}(f)E_f$  is solved with a mixed-integer solver [30]. The iso-parameter curves of  $u$  and  $v$  induce a quad mesh (see Fig. 9-middle, for example), where the mesh

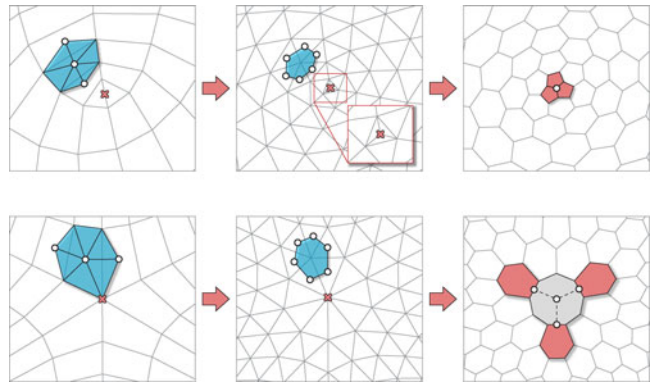


Fig. 10. Quad-to-hex conversion in the vicinity of field singularities with index  $\frac{1}{2}$  (top) and  $-\frac{1}{2}$  (bottom), respectively. Left: splitting each face of the quad mesh along the computed line field. Middle: the resulting triangulation. Right: a PH mesh is obtained by performing the tangent duality on the triangulation. Collapsing the triangle (top) result in a triple of pentagons (in red), while splitting the 9-polygon (bottom) result in a triple of heptagons (in red).

edges are aligned with principal directions of the surface and the edge sizes take the desired anisotropy. To obtain a mesh with a simple quad patch layout, we impose additional constraints in the parameterization for aligning the singularities as much as possible, i.e., enforcing some pair of field singularities to have the same  $u$ - or  $v$ - parameter.

## 4.3 Quad Mesh Triangulation

In Fig. 10, splitting each face of the anisotropic quad mesh at its center will produce a triangulation, which is an ideal triangulation by construction (see Fig. 9-right for example). Note that this simple splitting rule leads to a topologically valid triangulation as long as the quad mesh does not contain interior odd-valence vertices. Our quad mesh always splits into a valid triangulation, as its interior vertices can only be of three types, i.e., valence-2 at singularity of index  $\frac{1}{2}$ , valence-4 (regular vertex), and valence-6 at singularity of index  $-\frac{1}{2}$ . Fig. 10-middle shows the triangulation around these two kinds of singularities.

## 5 COMPUTING DUPIN-REGULAR PH MESHES

Theoretically, once an ideal triangulation  $T$  of the surface  $S$  is computed, it can easily be converted to a Dupin-regular PH mesh via tangent duality, as any valence-6 vertex of  $T$  corresponds to a planar hexagon under the duality transformation. However, there are two degenerate cases that have to be addressed in practice.

### 5.1 Handling Umbilical Regions ( $\kappa_1 \approx \kappa_2$ )

As one might have noticed, in each umbilical region,  $T$  contains a valence-3 (resp. valence-9) vertex at the field singularity of index  $\frac{1}{2}$  (resp.  $-\frac{1}{2}$ ), as shown in Fig. 10-middle, which would result in a triangle (resp. nonagon) in the final PH mesh. By collapsing the triangle (resp. splitting the nonagon), we obtain a trio of pentagons (resp. heptagons), indicated by the faces in red in Fig. 10-right. These non-hexagonal faces are necessary for compensating the Gaussian curvature of the surface and in general cannot be avoided. For example, when paneling a closed genus-0 surface (Euler characteristic  $\chi = 2$ ) with a hexagonal mesh  $H$  containing only valence-3 vertices,

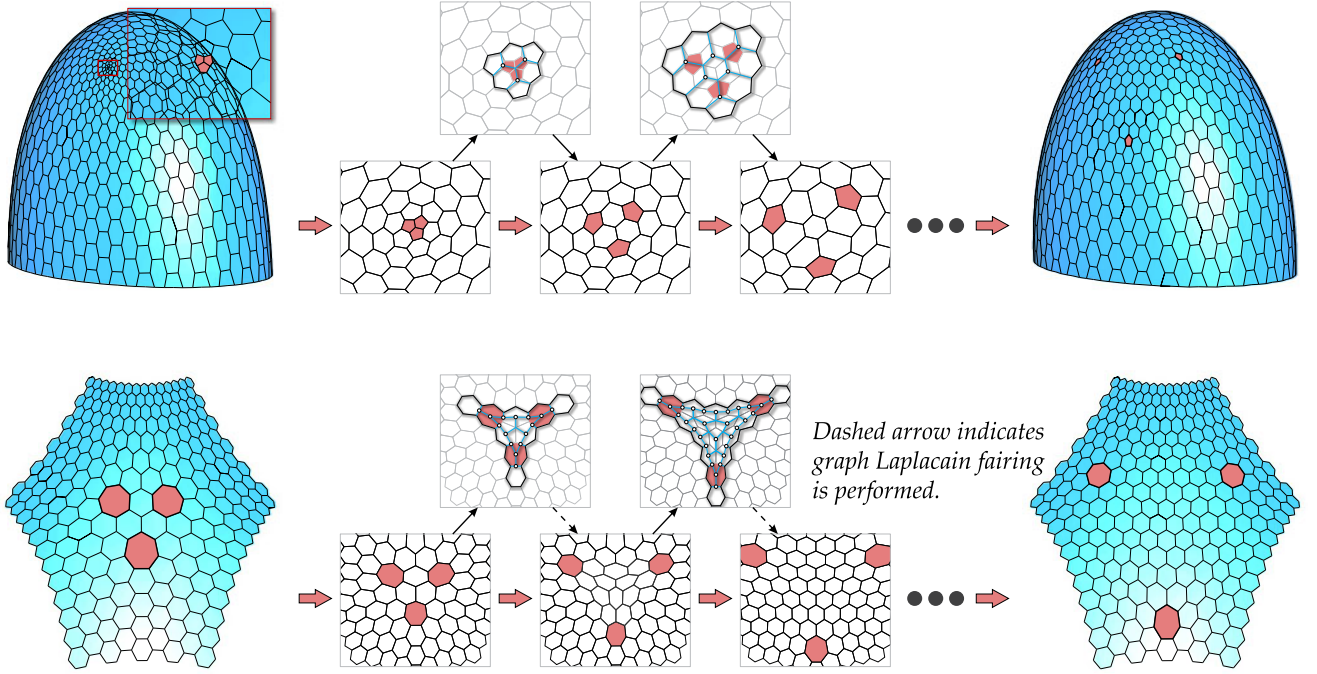


Fig. 11. (Top): Performing seven iterations of the pentagon diverging operator produces hexagon tiling with more uniform faces (pentagons are shaded in red). (Bottom): Performing three iterations of the heptagon diverging operator produces hexagon tiling with more uniform faces (heptagons are shaded in red). The planarity error of the mesh is retrieved via optimization.

$H$  cannot be free of non-hexagonal faces. If we further require the non-hexagonal faces to be pentagons or heptagons, it is not difficult to see that the number of pentagons  $N_5$  and heptagons  $N_7$  in  $H$  are subject to  $N_5 - N_7 = 12$ , according to *Euler's polyhedral formula*. In the viewpoint of an  $N$ -symmetry field [20], [31], [32], a pentagon (resp. heptagon) characterizes the field singularity of index  $\frac{1}{6}$  (resp.  $-\frac{1}{6}$ ). Given an  $N$ -symmetry field on a closed surface  $S$ , the sum of the singularity indices equals the Euler characteristic of  $S$ . This also indicates that hexagonal tiling  $H$  (with valence-3 vertices only) of genus-0 surface  $S$  has a minimum of 12 pentagons (e.g., a soccer ball has 12 pentagons and 20 hexagons).

However, the faces of a PH mesh  $H$  present a non-uniform pattern in the umbilical regions: see Fig. 11-left, the faces are either very small and cluttered around the singularity of index  $\frac{1}{2}$  (top), or very big and sparse around the singularity of index  $-\frac{1}{2}$  (bottom). Such non-uniform face patterns are desirable. Moreover, they bring about difficulties in the physical fabrication. To deal with these non-uniform face patterns in the umbilical regions, we propose two novel topological operators, *pentagon diverging* and *heptagon diverging*, for locally editing the connectivity of  $H$ .

*Pentagon diverging*. Around a singularity of index  $\frac{1}{2}$ , we have developed a topological operator for collapsing the cluttered small hexagons. Fig. 11-top illustrates the operator on  $H$ : we first identify the region  $R$  surrounded by a trio of pentagons; we then collapse the hexagons and the three pentagons located at  $R$ 's boundary, and re-tile the interior of  $R$  to construct topologically valid hexagon tiling. This operator amounts to collapsing a number of hexagons and pushing the trio of pentagons to diverge by one more ring of faces - hence the name.

*Heptagon diverging*. Likewise, around a singularity of index  $-\frac{1}{2}$ , we have developed an operator for splitting the sparse big hexagons. Fig. 11-bottom illustrates the operator

on  $H$ : we first identify the region  $R$  surrounded by a triple of heptagons; we then split the hexagons and the three heptagons located at  $R$ 's boundary, and re-tile the interior of  $R$  to construct a topologically valid hexagon tiling. This operator amounts to padding a number of hexagons into  $R$ 's boundary and pushing the triple of heptagons to diverge by one more ring of faces - hence the name.

*Remark*. These two operators are local operators that modify the mesh connectivity only around the field singularities without introducing additional non-hexagonal faces. Executing them a few times, followed by graph-based Laplacian smoothing, leads to a hexagonal mesh with more uniform face patterns (see Fig. 11-right). One might be concerned with face planarity after performing these operators. We stress that the affected faces are located at the umbilical regions of the surface where the PH faces have more rotational freedom, as the Dupin conics are nearly circles ( $\kappa_1 \approx \kappa_2$ ). Thus, it is not difficult to obtain the face planarity by locally perturbing the vertices via optimization (discussed in Section 5.3). See the planarity error (PE) of the optimized mesh in Table 1.

TABLE 1  
Planarity Error of the PH Meshes

Model	#face	$PE_{max}$	$PE_{avg}$
Fig. 11-top right	817	$7.84 \times 10^{-9}$	$1.08 \times 10^{-10}$
Fig. 11-bottom right	241	$1.45 \times 10^{-4}$	$8.46 \times 10^{-5}$
Fig. 12-right	1248	$2.09 \times 10^{-14}$	$3.78 \times 10^{-16}$
Fig. 13-right	330	$4.10 \times 10^{-4}$	$1.21 \times 10^{-4}$
Fig. 16	1120	$8.71 \times 10^{-14}$	$5.03 \times 10^{-15}$
Fig. 17-left	1557	$1.22 \times 10^{-4}$	$5.97 \times 10^{-7}$
Fig. 17-right	1316	$4.16 \times 10^{-14}$	$2.33 \times 10^{-16}$
Fig. 18-left	2124	$1.05 \times 10^{-4}$	$2.08 \times 10^{-5}$
Fig. 18-right	1377	$3.38 \times 10^{-4}$	$7.34 \times 10^{-5}$
Fig. 20	1302	$4.18 \times 10^{-3}$	$2.99 \times 10^{-4}$

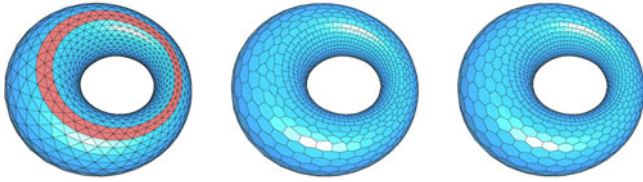


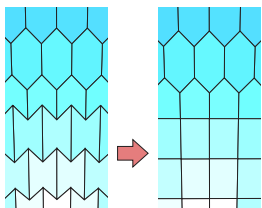
Fig. 12. Left: Triangles in the parabolic regions are shaded in red. Middle: The tangent duality of those triangles becomes numerically unstable, producing misshaped PH faces. Right: Centroids are taken as duals of those triangles, producing well-shaped hexagons. The planarity error of the mesh is retrieved via optimization, see Table 1.

## 5.2 Handling Parabolic Regions ( $K \approx 0$ )

Freeform surfaces often contain parabolic curves (formed by parabolic points  $K = 0$ ), and a numerical issue arises in constructing the tangent dual for the triangles (e.g., the red triangles in Fig. 12-left) in the parabolic regions, i.e., in the vicinity of those curves. For such a triangle  $t$ , the three tangent planes  $\Gamma_1$ ,  $\Gamma_2$ , and  $\Gamma_3$  at its vertices are nearly parallel and computing their intersection point becomes numerically unstable. As a result, awfully-shaped or even self-intersecting PH faces arise (Fig. 12-middle). In this case, it is very difficult to recover a Dupin-regular PH mesh from such an initialization. A practical way of dealing with this problem is to take the centroid of  $t$  as its dual point, which is a reasonable approximation to the tangent dual of  $t$ , since the plane to which  $t$  belongs almost coincides with  $\Gamma_1$ ,  $\Gamma_2$ , or  $\Gamma_3$ . Fig. 12-right shows that a fairing convex-concave hexagon transition is recovered due to the employment of face centroids.

Another issue is that the parabolic lines of surface  $S$ , separating the  $K > 0$  and  $K < 0$  regions of  $S$  (Fig. 13-left), do not generally align with the curvature lines of  $S$ . As a result, the transition between convex and concave hexagons is aesthetically unpleasant (Fig. 13-middle). In this case, for the triangles within the region (the quad patch highlighted in Fig. 13-left) where the parabolic line crosses curvature lines, we also replace the tangent dual with the face centroid so as to achieve a better convex/concave hexagon transition (Fig. 13-right). In our implementation, we manually select the regions affected by parabolic lines for easy control.

*Remark.* In parabolic regions, due to the employment of centroids, the planarity of the dualized hexagons in general cannot be guaranteed. However, we stress that the affected faces are not far from being planar since  $K \approx 0$ . In Section 5.3, we shall present an optimization framework for locally perturbing the vertices so as to achieve exact face planarity.



*Hybrid PH-PQ meshes.* In the areas of a surface where  $K < 0$ , the PH faces are constrained to take concave shapes, which are sometimes not preferred in the fabrication of architectural surfaces, as they may cause cracks due to the large stress concentration on concave vertices [33]. When

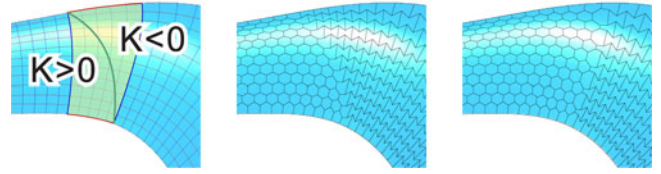


Fig. 13. Left: The highlighted region shows the area where the parabolic line (in green) crosses the curvature lines (in blue and red). Middle: Directly constructing the tangent dual results in unpleasant hexagon transitions. Right: Centroid duality is employed for the triangles within the highlighted region, producing pleasant convex-concave hexagon transitions. The planarity error of the mesh is retrieved via optimization, see Table 1.

concave faces need to be avoided for such reasons, we propose re-tiling the  $K < 0$  regions with planar quad faces and construct a so-called *hybrid PH-PQ* mesh (see the inset). The operation is as follows: (1) identify any concave hex and split it into 2 quads at the vertex whose included angle is bigger than  $\pi$  (Fig. 14a) automatically; (2) smooth the generated quads by applying the mesh fairing algorithm [34] (Fig. 14b); (3) coarsen the quads by removing a half number of grid lines along the splitting direction (Fig. 14c). The planarity of the hybrid mesh can be easily achieved by optimization (see Table 1), as the edges of the quad faces are aligned with the principal directions of the surface. Fig. 18 shows two architectural designs paneled by such hybrid PH-PQ meshes. The resulting hybrid mesh does not contain any face with concave corners and hence the structural stability of the mesh is greatly improved.

## 5.3 Optimization

For an ideal triangulation  $T$  on surface  $S$  that contains no umbilical or parabolic points, the tangent duality provides a fast and precise method for turning  $T$  into a Dupin-regular PH mesh. However, as we discussed, the face planarity is traded for mesh aesthetics, due to the execution of topological operators in the umbilical regions as well as the employment of centroids in the parabolic regions. Thus, for the above initialized PH mesh  $H$ , we shall devise an optimization framework for reinforcing the face planarity while preserving the mesh fairness and shape fidelity.

*Face planarity.* In order to have faces with exact planarity, we propose the planarity constraint for a  $N$ -polygon  $f = v_0v_1 \dots v_{N-1}$ : a plane  $p := \hat{\mathbf{n}}_f \cdot \mathbf{x} + d_f = 0$  ( $\hat{\mathbf{n}}_f$  is the unit normal of  $p$ ) is first identified to fit  $f$  in the least-square sense. The planarity of  $f$  could be attained by requiring the

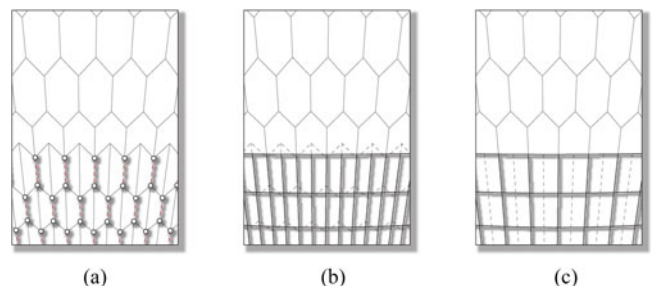


Fig. 14. (a): Split any concave hex at its concave vertex (included angle  $> \pi$ ). (b): Smooth the generated quads. (c): Coarsen the quads by removing a half number of grid lines along the splitting direction.

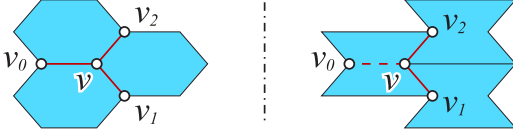


Fig. 15. Quasi-Laplacian fairing for hexagon tiling in the case of  $K > 0$  (left) and  $K < 0$  (right).

distance between every vertex of  $f$  and the fitted plane  $p$  to be zero, which amounts to forcing:

$$C_{f,i} := \hat{\mathbf{n}}_f \cdot \mathbf{v}_i + d_f = 0, \quad i = 0, 1, \dots, N - 1. \quad (1)$$

*Fairness of PH meshes.* In order to preserve the mesh fairness during the planarization, we generalize the graph Laplacian operator based on simple heuristics and introduce the *quasi-Laplacian fairing* energy on PH meshes. For a vertex  $v$ , its fairing error is naturally defined as

$$E_{fair} = \sum_i \|\mathbf{v} - \bar{\mathbf{v}}_i\|^2,$$

where  $\bar{\mathbf{v}}_i$  is the average position of  $v$ 's neighbors. In the case of  $K > 0$ , the neighbors are chosen as the vertices directly connected with  $v$  (Fig. 15-left); while in the case of  $K < 0$ , a modification needs to be made and the neighbors involved for computing  $\bar{\mathbf{v}}_i$  are shown in Fig. 15-right. It is trivial to verify that, in  $K < 0$  regions, this modification preserves the hexagonal concaveness and attempts to produce Dupin quasi-regular hexagons. In our experiments, the concavity of a vertex on face  $f$  is detected by checking whether  $\mathbf{n}_f \cdot \mathbf{n}_e$  is less than 0.1. Here,  $\mathbf{n}_f$  is the face normal and  $\mathbf{n}_e$  is the normalized cross-product of edge vectors connected to this vertex.

*Closeness term.* To ensure minimal vertex perturbation and surface distortion, we minimize the *original* energy  $E_{orig}$  and *closeness* energy  $E_{dist}$  of every vertex  $v_i$  in the optimization:

$$E_{orig} = \sum_i \|\mathbf{v}_i - \mathbf{v}_{i,0}\|^2,$$

$$E_{dist} = \sum_i \text{dist}^2(\mathbf{v}_i, \mathbf{S}),$$

$\mathbf{v}_{i,0}$  is the initial position of  $v_i$  and  $\text{dist}$  is the distance between  $v_i$  and its foot point on the underlying surface  $\mathbf{S}$ .

In summary, the optimization framework is formulated as

$$\min E_{PH} = w_{fair} E_{fair} + w_{orig} E_{orig} + w_{dist} E_{dist}, \quad (2)$$

subject to the face planarity constraints in Eq. (1) ( $w_{fair} = 1.0$ ,  $w_{orig} = 0.1$ ,  $w_{dist} = 0.1$  in our experiments). Here the variables are the positions of vertices, and  $\{\hat{\mathbf{n}}_f, d_f\}$  for each face. We solve this *constrained quadratic optimization* problem by using the augmented Lagrangian method [35].

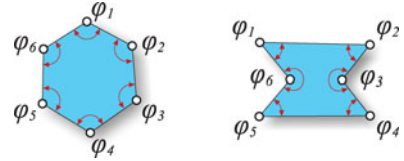
## 6 OFFSETS OF PH MESHES

In addition to face planarity, the offset properties are also very useful from the view of the physical realization of multi-layer freeform architectures since they serve as the basis for constructing the supporting structures and geometrically optimal mesh nodes. Pottmann et al. [6] propose the concept of *mesh parallelism* and studied different offset meshes. Two meshes  $\mathcal{M}$  and  $\mathcal{M}'$  are *parallel* if  $\mathcal{M}$  and  $\mathcal{M}'$  have the same combinatorics and the corresponding edges are parallel. Mesh parallelism is only used for meshes with

planar faces, thus in this section all meshes are assumed to have planar faces. Clearly, the corresponding faces of parallel meshes lie in parallel planes.  $\mathcal{M}$  and  $\mathcal{M}'$  are offset from each other if they are parallel and the distance between them is constant throughout the mesh. Since there are different ways of defining the *distance*, i.e., face distance, vertex distance, and edge distance, we distinguish *face*, *vertex*, and *edge offsets* according to the distance type that is used. The face offset property of polyhedral meshes has been studied thoroughly [2]. In this section, we are interested in developing practical optimization methods for the computation of *vertex* and *edge offsets*, respectively.

### 6.1 Vertex Offset

A polygonal mesh has an exact vertex offset if and only if it is *quasi-circular* [36], i.e., each face has a parallel circular polygon inscribed in a unit circle. An equivalent angle criterion is: a planar quad is quasi-circular, if and only if the four angles enclosed by its four edges have the property  $\varphi_1 + \varphi_3 = \varphi_2 + \varphi_4 = \pi$ . Likewise, a planar hex is quasi-circular if and only if the six angles enclosed by its six edges have the property  $\varphi_1 + \varphi_3 + \varphi_5 = \varphi_2 + \varphi_4 + \varphi_6 = 2\pi$ , which applies to both convex and concave cases (see the right inset). To compute a PH or PH-PQ mesh  $\mathcal{M}$  that is quasi-circular, we add this angle constraint into the constraint system of (2) for every face of  $\mathcal{M}$ . After obtaining a quasi-circular PH mesh, one can construct its vertex offset mesh by computing its Gaussian image [36].



### 6.2 Approximate Edge Offset

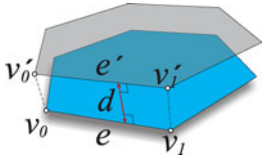
Compared to a face or vertex offset, the edge offset property is rather restrictive: PH meshes possessing face or vertex offsets are capable of approximating an arbitrary shape, which is no longer the case with edge offset meshes [6]. As a matter of fact, the possible shapes that could be approximated by PH meshes with exact edge offsets are still unknown at the present time. Therefore, we provide an optimization algorithm for computing the *approximate* edge offset  $\mathcal{M}'$  of a given mesh  $\mathcal{M}$ , i.e., the corresponding edges of  $\mathcal{M}$  and  $\mathcal{M}'$  have an approximately constant distance.

Given a PH or PH-PQ mesh  $\mathcal{M}$ , a mesh  $\mathcal{M}'$  is first constructed by translating each vertex  $v$  of  $\mathcal{M}$  along the normal direction at  $v$  by a user-specified distance  $d$ , which initializes an edge offset mesh. We then perturb the vertex positions of both  $\mathcal{M}$  and  $\mathcal{M}'$  at the same time so that  $\mathcal{M}$  and  $\mathcal{M}'$  become edge offsets of each other as much as possible.

*Parallelism constraint.* During the optimization, the parallelism of any directed edge  $e = \overrightarrow{v_0 v_1}$  of  $\mathcal{M}$  and its correspondence  $e' = \overrightarrow{v'_0 v'_1}$  of  $\mathcal{M}'$  is forced by imposing the constraints (see the right inset for notation):

$$C_{para} := (\mathbf{v}_1 - \mathbf{v}_0) \times (\mathbf{v}'_1 - \mathbf{v}'_0) = \mathbf{0}, \quad (3)$$

where " $\times$ " stands for the cross product.



*Edge distance term.* For any pair  $e$  and  $e'$ , their distance is optimized as close to  $d$  as possible by minimizing:

$$E_{edge} := \left[ \left( \frac{(\mathbf{v}_1 - \mathbf{v}_0) \cdot (\mathbf{v}'_0 - \mathbf{v}_0)}{\|\mathbf{v}_1 - \mathbf{v}_0\|} \right)^2 + d^2 - \|\mathbf{v}'_0 - \mathbf{v}_0\|^2 \right]^2,$$

where  $\frac{(\mathbf{v}_1 - \mathbf{v}_0)}{\|\mathbf{v}_1 - \mathbf{v}_0\|} \cdot (\mathbf{v}'_0 - \mathbf{v}_0)$  is the projection of  $\overrightarrow{v_0 v'_0}$  onto  $\overrightarrow{v_0 v_1}$ .

To summarize, the edge offset optimization is formulated as

$$\min E_f(\mathcal{M}) + E_f(\mathcal{M}') + w_{edge} E_{edge}, \quad (4)$$

subject to face planarity constraints (1) and edge parallel constraints (3) on both meshes.

Compared with the optimization strategy in [6], our optimization does not involve the Gaussian image and is carried out on  $\mathcal{M}'$  as well as the original mesh  $\mathcal{M}$ , producing two planar parallel meshes with an approximately constant edge-edge distance. The effectiveness of our method is demonstrated by experiments in Section 7.

## 7 EXPERIMENTS

The efficacy of our method is demonstrated on a variety of architectural shapes. All the experiments are conducted on a 2.4 GHz Intel Xeon CPU with 4 GB of RAM and the planarity errors of the PH meshes are reported in Table 1. All the models are normalized to have a unit bounding box for measuring numerical errors. The planarity error of each face  $f$  is evaluated as the largest distance between any of its vertices and its fitting plane  $p$ .  $PE_{max}$  and  $PE_{avg}$  stand for the maximum and average planarity error  $PE$  among all faces of a mesh.

Fig. 17 demonstrates two architectural designs paneled by PH meshes where both the face planarity (see Table 1) and mesh aesthetics are well achieved. As demonstrated, the PH faces are nearly Dupin regular/quasi-regular hexagons aligned with the principal directions, and they present a pleasant transition when crossing the parabolic lines. Moreover, the PH faces in the umbilical regions exhibit a uniform pattern thanks to our topological operations.

*Subdivision based modeling.* For a given surface  $S$ , computing a faithful discretization of the principal curve network on  $S$  is the key for paneling  $S$  with aesthetic PH meshes. In addition to paneling the given freeform shapes with PH meshes, the modeling/design of such architecture shapes is also in great demand. As previously mentioned, circular PQ meshes approximating an underlying surface  $S$  are discretizations of the principal curve network of  $S$  [37]. Making a quad mesh  $Q$  circular amounts to requiring every face  $f$  of  $Q$  to be inscribed in a circle, that is, imposing a constraint  $\phi_1 + \phi_3 = \phi_2 + \phi_4 = \pi$  on  $f$  into the optimization in Section 5.3.  $\phi_1 \sim \phi_4$  are the four inner angles of  $f$  in consecutive order. Inspired by this observation, we present a modeling framework by combining the circular PQ mesh optimization with

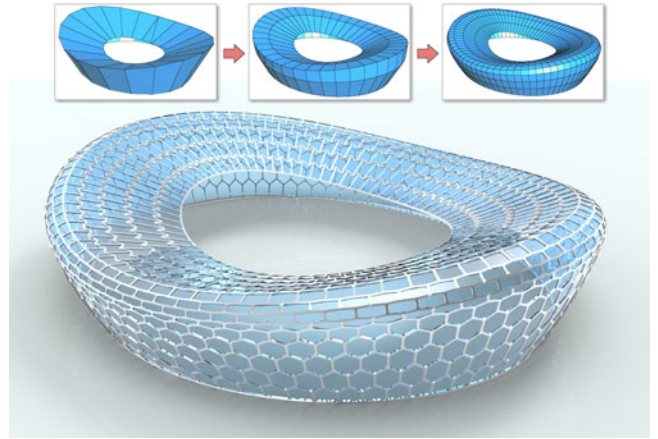


Fig. 16. A stadium shape designed by our subdivision-optimization method: a sequence of circular PQ meshes are produced, and a PH mesh is then constructed.

a quad-based subdivision scheme like Catmull-Clark in an alternating manner: starting from a very coarse circular PQ mesh  $Q_0$  (optimize it if it is not circular), we subdivide it once and then optimize the subdivided mesh  $Q_1$  to be circular. These two steps are iteratively executed to generate a hierarchical sequence of circular PQ meshes  $Q_i$ , and the iteration stops if a circular PQ mesh  $Q_n$  of reasonable density is obtained, serving as the discrete principal curve network of the resulting surface.

Note that the initial quad mesh  $Q_0$  is required to be free of (interior) odd-valence vertices, since we would otherwise have difficulties converting  $Q_n$  to a triangulation (see Section 4.3). Another issue we need to consider is that the faces of  $Q_n$  usually do not have the desired anisotropy. To optimize the face anisotropy of  $Q_n$ , we suggest performing the quad mesh *re-sampling* approach as proposed in [38], which optimizes the sampling rate of the mesh edges without changing their directions. This subdivision-based approach enables the user to express and edit their design intention at an early stage, thus facilitating the design process. Fig. 16 demonstrates a PH mesh modeled using our subdivision-based method.

*Various offset meshes with supporting structures.* Fig. 18-right shows an example of a quasi-circular hybrid PH-PQ mesh (i.e., each face has a parallel circular polygon inscribed in a unit circle), thus possessing exact vertex offsets. Fig. 17-right shows an example of a PH mesh that supports an approximate edge offset. The beam width  $d$  is specified as 0.02 in the optimization. After the optimization converges, the largest and smallest edge-edge distance is 0.020095 and 0.019776, respectively (the deviation is within 1.1 percent of the specified  $d$ ). We also compare our result with the existing approach of [6], where the approximate edge offset is obtained by finding a parallel mesh approximating the unit sphere. Fig. 19 shows the Gaussian images  $(\mathcal{M} - \mathcal{M}')/d$  from these methods. Visualizing Gaussian images is an easy way to illustrate the approximate edge-offset property. If all the edges of a Gaussian image are tangential to the unit sphere, the corresponding PH mesh has the exact edge-offset property. It is clear that the result from [6]'s method contains edges that have a large edge-offset to the unit-sphere, so our result approximates the unit sphere much better.

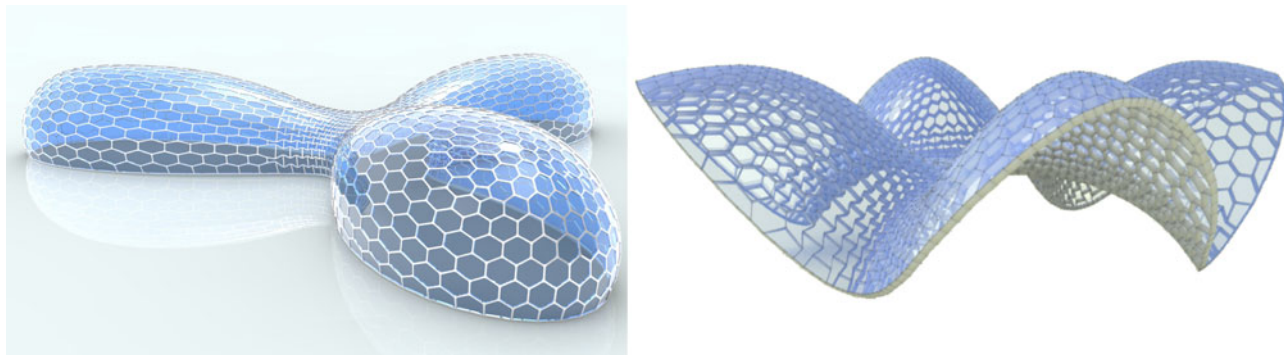


Fig. 17. Architectural designs paneled by planar hexagonal (PH) meshes generated by our method. The right mesh supports an approximate edge offset.

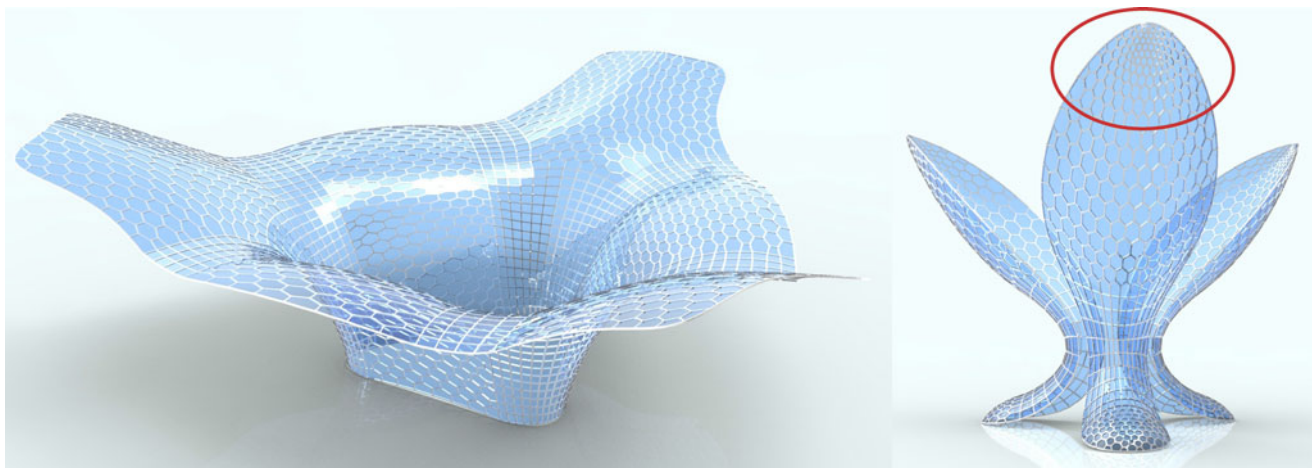


Fig. 18. Two architectural designs paneled by hybrid PH-PQ meshes. The right mesh possesses the vertex offset property.

## 8 CONCLUSION

PH meshes feature many desirable properties and have received increasing attention in architectural design and fabrication. Although several optimization methods have been proposed for planarizing polygonal meshes [17], [18], the issue of providing a proper initialization has largely been overlooked. We stress that the face planarity and mesh aesthetics can be conflicting goals if the initial mesh is not properly discretized from the underlying surface. In this paper, we solved the problem of computing proper initial meshes for computing PH meshes by introducing the optimal shape of PH faces and concluding the ideal triangulation that corresponds to an aesthetic PH mesh under

tangent duality. We also provided a practical framework for computing such ideal triangulations and addressed how to handle umbilical regions and parabolic regions on freeform surfaces. Finally, we discussed several practical issues in the design and fabrication of PH meshes, e.g., providing a subdivision-based modeling framework for facilitating the design process of PH meshes and proposing the use of hybrid PH-PQ meshes to improve the structural stability.

In our framework, computing an ideal triangulation with curvature-aligned anisotropic triangles is the key to generating a Dupin-regular PH mesh. Existing anisotropic triangulation techniques like [39], [40] are not employed, as they often produce meshes with an uncontrolled number of singular vertices, which would be dual to non-hexes in the final PH mesh. Nieser et al. [20] propose a hexagonal parameterization method that can be used to compute semi-regular hexagonal meshes. However, their method does not apply to an anisotropic case and thus has difficulties in achieving face planarity and mesh aesthetics at the same time.

Paneling a freeform surface with aesthetic PH meshes is indeed a challenging problem, in that the face shapes are highly constrained by the surface geometry. Take the shape in Fig. 18-right for example, the faces in the umbilical region (highlighted in the red circle) are still crowded even after performing our topological operations. Moreover, we assume the input surfaces in our method present smooth curvature fields (that is usually the case in architectural design). However, given a surface containing many intersected parabolic curves, it is still hard to compute an

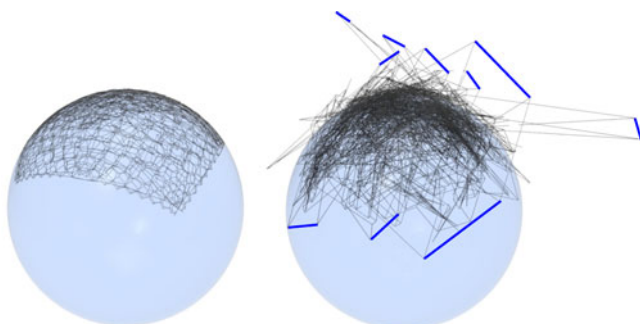


Fig. 19. Left: the Gaussian image generated by our method:  $(\mathcal{M} - \mathcal{M}')/d$ . Right: the Gaussian image computed by the algorithm of [6]. The edges that have large offset distances to the unit sphere are colored in blue.

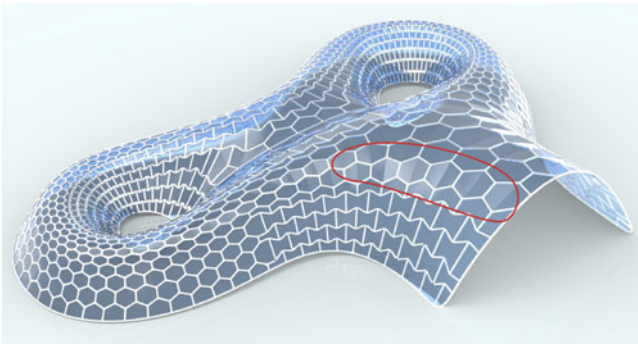


Fig. 20. Paneling a PH mesh on a complex shape.

aesthetic PH mesh paneling on it with our method. Fig. 20 demonstrates such a shape, which contains sharp features (edges connecting the two holes) as well as several intersected parabolic lines. In order to obtain an aesthetic PH layout on it, we have tried to align the parabolic lines with the curvature lines and increase the weight of the fairing energy during the optimization; however the face planarity would have to be compromised a little. See the circled region for non-planar faces as well as the planarity error in Table 1. Hence, how to locally perturb a surface to suppress parabolic lines remains an interesting problem for future research.

Taking account of static equilibrium is important in real architectural construction. For PQ meshes, Vouga et al. propose a way of designing self-supporting PQ meshes where the thrust network built on the mesh reaches static equilibrium [41]. This nice self-supporting property is well suited to a steel-glass structure, especially where steel-beams bear forces only. It would be interesting to embed self-supporting property into PH mesh design in the future.

It is worth mentioning that we focus on approximating a given shape with a PH mesh in this paper and do not consider how to minimize the number of different PH panels for reducing the real construction cost. It is possible to extend techniques presented in [4], [42], [43] and use our PH meshes as an initialization to cut the cost while still approximating the original shape.

## ACKNOWLEDGEMENTS

The work of Wenping Wang was partially supported by the National Basic Research Program of China (2011CB302400), NSFC (61272019) and the Research Grant Council of Hong-Kong (718209, 718010, 718311, 717012).

## REFERENCES

- [1] J. Glymph, D. Shelden, C. Ceccato, J. Mussel, and H. Schober, "A parametric strategy for free-form glass structures using quadrilateral planar facets," *Autom. Construction*, vol. 13, pp. 187–202, 2004.
- [2] Y. Liu, H. Pottmann, J. Wallner, Y.-L. Yang, and W. Wang, "Geometric modeling with conical meshes and developable surfaces," *ACM Trans. Graph.*, vol. 25, pp. 681–689, 2006.
- [3] H. Pottmann, A. Asperl, M. Hofer, and A. Kilian, *Architectural Geometry*. Stockton Dr., PA, USA: Bentley Inst. Press, 2007.
- [4] M. Eigensatz, M. Kilian, A. Schiffner, N. J. Mitra, H. Pottmann, and M. Pauly, "Paneling architectural freeform surfaces," *ACM Trans. Graph.*, vol. 29, pp. 45:1–45:10, 2010.
- [5] B. Grunbaum and G. C. Shephard, *Tilings and Patterns*. San Francisco, CA, USA: Freeman, 1987.
- [6] H. Pottmann, Y. Liu, J. Wallner, A. Bobenko, and W. Wang, "Geometry of multi-layer freeform structures for architecture," *ACM Trans. Graph.*, vol. 26, pp. 65:1–65:12, 2007.
- [7] M. Zadrevac, A. Schiffner, and J. Wallner, "Designing quad-dominant meshes with planar faces," *Comput. Graph. Forum*, vol. 29, no. 5, pp. 1671–1679, 2010.
- [8] A. Bobenko, H. Pottmann, and J. Wallner, "A curvature theory for discrete surfaces based on mesh parallelity," *Math. Annalen*, vol. 348, pp. 1–24, 2010.
- [9] Y. Liu, W. Xu, J. Wang, L. Zhu, B. Guo, F. Chen, and G. Wang, "General planar quadrilateral mesh design using conjugate direction field," *ACM Trans. Graph.*, vol. 30, pp. 140:1–140:10, 2011.
- [10] H. Coxeter, *Introduction to Geometry*, 2nd ed. Hoboken, NJ, USA: Wiley, 1989.
- [11] B. Cutler and E. Whiting, "Constrained planar remeshing for architecture," in *Proc. Graph. Interface*, 2007, pp.11–18.
- [12] W. Wang, Y. Liu, D.-M. Yan, B. Chan, R. Ling, and F. Sun, "Hexagonal meshes with planar faces," The Univ. Hong Kong, Pokfulam, Hong Kong, Tech. Rep. TR-2008-13, 2008.
- [13] A. I. Bobenko, T. Hoffmann, and B. A. Springborn, "Minimal surfaces from circle patterns: Geometry from combinatorics," *Am. Math.*, vol. 164, no. 1, pp. 231–264, 2006.
- [14] C. Müller and J. Wallner, "Oriented mixed area and discrete minimal surfaces," *Discrete Comput. Geom.*, vol. 43, no. 2, pp. 303–320, 2010.
- [15] W. Wang and Y. Liu, "A note on planar hexagonal meshes," *Non-linear Computational Geometry*. New York, NY, USA: Springer-Verlag, 2009, pp. 221–233.
- [16] C. Troche, "Planar hexagonal meshes by tangent plane intersection," in *Proc. Adv. Archit. Geom. Conf.*, 2008, pp. 57–60.
- [17] H. Zimmer, M. Campen, R. Herkrath, and L. Kobbelt, "Variational tangent plane intersection for planar polygonal meshing," in *Proc. Adv. Archit. Geom.*, 2012, pp. 319–332.
- [18] R. Poranne, E. Ovreiu, and C. Gotsman, "Interactive planarization and optimization of 3D meshes," *Comput. Graph. Forum*, vol. 31, pp. 152–163, 2013.
- [19] Y.-K. Lai, S.-M. Hu, and R. R. Martin, "Surface mosaics," *Vis. Comput.*, vol. 22, no. 9–11, pp. 604–611, 2006.
- [20] M. Nieser, J. Palacios, K. Polthier, and E. Zhang, "Hexagonal global parameterization of arbitrary surfaces," *IEEE Trans. Vis. Comput. Graph.*, vol. 18, no. 6, pp. 865–878, Jun. 2012.
- [21] A. Sheffer, E. Praun, and K. Rose, "Mesh parameterization methods and their applications," *Found. Trends Comput. Graph. Vis.*, vol. 2, no. 2, pp. 105–171, 2006.
- [22] D. Cohen-Steiner, P. Alliez, and M. Desbrun, "Variational shape approximation," *ACM Trans. Graph.*, vol. 23, pp. 905–914, 2004.
- [23] H. Almegaard, A. Bagger, J. Gravesen, B. Jüttler, and Z. Šir, "Surfaces with piecewise linear support functions over spherical triangulations," in *Proc. 12th IMA Int. Conf. Math. Surfaces XII*, 2007, vol. 4647, pp. 42–63.
- [24] M. D. Carmo, *Differential Geometry of Curves and Surfaces*. Englewood Cliffs, NJ, USA: Prentice-Hall, 1976.
- [25] D. J. Struik, *Lectures on Classical Differential Geometry*, 2nd ed. New York, NY, USA: Dover, 1988.
- [26] K. Crane, M. Desbrun, and P. Schröder, "Trivial connections on discrete surfaces," *Comput. Graph. Forum*, vol. 29, no. 5, pp. 1525–1533, 2010.
- [27] B. Smyth and F. Xavier, "A sharp geometric estimate for the index of an umbilic on a smooth surface," *Bull. London Math. Soc.*, vol. 24, pp. 176–180, 1992.
- [28] A. Hertzmann and D. Zorin, "Illustrating smooth surfaces," in *Proc. 27th Annu. Conf. Comput. Graph. Interactive Tech.*, 2000, pp. 517–526.
- [29] F. Kälberer, N. Matthias, and K. Polthier, "QuadCover—Surface parameterization using branched coverings," *Comput. Graph. Forum*, vol. 26, pp. 375–384, 2007.
- [30] D. Bommers, H. Zimmer, and L. Kobbelt, "Mixed-integer quadrangulation," *ACM Trans. Graph.*, vol. 28, pp. 77:1–77:10, 2009.
- [31] J. Palacios and E. Zhang, "Rotational symmetry field design on surfaces," *ACM Trans. Graph.*, vol. 26, pp. 55:1–55:10, 2007.
- [32] N. Ray, B. Vallet, W. C. Li, and B. Lévy, "N-symmetry direction field design," *ACM Trans. Graph.*, vol. 27, pp. 10:1–10:13, 2008.
- [33] A. Bagger, "Plate shell structures of glass," Ph.D. dissertation, Dept. Civil Eng., Technical Univ. Denmark, Copenhagen, Denmark, 2010.
- [34] G. Taubin, "A signal processing approach to fair surface design," in *Proc. 22nd Annu. Conf. Comput. Graph. Interactive Tech.*, 1995, pp. 351–358.

- [35] J. Nocedal and S. J. Wright, *Numerical Optimization*. New York, NY, USA: Springer-Verlag, 1999.
- [36] Y. Liu and W. Wang, "On vertex offsets of polyhedral surfaces," in *Proc. Adv. Archit. Geom. Conf.*, 2008, pp. 61–64.
- [37] R. R. Martin, J. De Pont, and T. J. Sharrock, "Cyclide surfaces in computer aided design," in *Proc. Conf. Organized Inst. Math. Appl. Math. Surfaces*, 1986, pp. 253–268.
- [38] Y. Li, W. Wang, R. Ling, and C. Tu, "Shape optimization of quad mesh elements," *Comput. Graph.*, vol. 35, no. 3, pp. 444–451, 2011.
- [39] F. Labelle and J. R. Shewchuk, "Anisotropic Voronoi diagrams and guaranteed-quality anisotropic mesh generation," in *Proc. 19th Annu. Symp. Comput. Geom.*, 2003, pp.191–200.
- [40] J.-D. Boissonnat, C. Wormser, and M. Yvinec, "Anisotropic Delaunay mesh generation," INRIA, Valbonne, France, Tech. Rep. RR-7712, 2011.
- [41] E. Vouga, M. Höbinger, J. Wallner, and H. Pottmann, "Design of self-supporting surfaces," *ACM Trans. Graph.*, vol. 31, pp. 87:1–87:11, 2012.
- [42] C.-W. Fu, C.-F. Lai, Y. He, and D. Cohen-Or, "K-set tilable surfaces," *ACM Trans. Graph.*, vol. 29, pp. 44:1–44:6, 2010.
- [43] M. Singh and S. Schaefer, "Triangle surfaces with discrete equivalence classes," *ACM Trans. Graph.*, vol. 29, pp. 43:1–43:6, 2010.



**Yufei Li** received the BEng degree in automation from the University of Science and Technology of China in 2006 and the PhD degree in computer science from The University of Hong Kong in 2012. He is a postdoctoral fellow in the Department of Computer Science at The University of Hong Kong. His research interests include computer graphics, geometric modeling, and architectural geometry.



**Yang Liu** received the bachelor's and master's degrees in computational mathematics from the University of Science and Technology of China, in 2000 and 2003, respectively, and the PhD degree in computer science from The University of Hong Kong in 2008. He is a researcher in the Internet Graphics Group at Microsoft Research Asia. After completing his PhD degree, he worked in Alice group at INRIA/LORIA as a post-doctoral researcher starting in 2008. He joined Microsoft Research Asia in 2010. His research interests include geometric modeling, computer-aided geometric design, and architectural geometry.



**Wenping Wang** is a professor of computer science at the University of Hong Kong. His research covers computer graphics, visualization, and geometric computing. He has recently focused on mesh generation and surface modeling for architectural design. He is a journal associate editor of *Computer Aided Geometric Design (CAGD)*, *Computers and Graphics (CAG)*, *IEEE Transactions on Visualization and Computer Graphics (TVCG)*, 2008-2012), *Computer Graphics Forum (CGF)*, and *IEEE Computer Graphics and Applications (CG&A)*. He has been the program chair of several international conferences, including Pacific Graphics 2003, ACM Symposium on Physical and Solid Modeling (SPM 2006), International Conference on Shape Modeling (SMI 2009), and the conference chair of Pacific Graphics 2012, SIAM Conference on Geometric and Physical Modeling 2013 (GD/SPM'13), and SIGGRAPH Asia 2013.

▷ For more information on this or any other computing topic, please visit our Digital Library at [www.computer.org/publications/dlib](http://www.computer.org/publications/dlib).